This is a peer-reviewed, accepted author manuscript of the following research article: Bradley, LJ & Wright, NG 2024, 'Characterization and performance of an optical-relay switching system for cost-effective multichannel sensing arrays', IEEE Sensors Journal, vol. 24, no. 12, pp. 19728-19735. https://doi.org/10.1109/JSEN.2024.3393762

Characterization and Performance of an Optical-Relay Switching System for Cost-Effective Multichannel Sensing Arrays

Luke J. Bradley and Nick G. Wright *Member, IEEE*

***Abstract*— Multi-sensor technology is now commonly used in many applications to monitor a wide range of complex systems. In many cases, the outputs from the individual sensors are multiplexed through relays or electronic switching systems into the detection and signal conditioning electronics so that only one set of measurement equipment is required. These switching systems are often very expensive and limited to relatively benign laboratory type environments. Within the work presented here, the performance of commercial off-the-shelf (COTS) optical relay ICs within a digital switching system are characterized to access their suitability in a cost-effective switching system. A low-cost (sub £30) optical-relay switch system (ORSS) is developed and characterized that achieves remote switching speeds of over 2800 switches/s. Combining the ORSS with a sourcemeter results in measurement speeds of up to 66 sensors/s with less than 1% error compared to measuring the sensors individually. Finally, in demonstrating the application of the ORSS, multiple temperature sensors were used to monitor the temperature profile of a microcontroller board where a clear temperature profile for the individual components and the printed circuit board (PCB) is measured. Hence demonstrating that this ultra-fast and cost-effective ORSS can be used for a wide area of applications including large-scale device characterization, monitoring multichannel sensors for workplace safety, or data acquisition in industry and academia.**

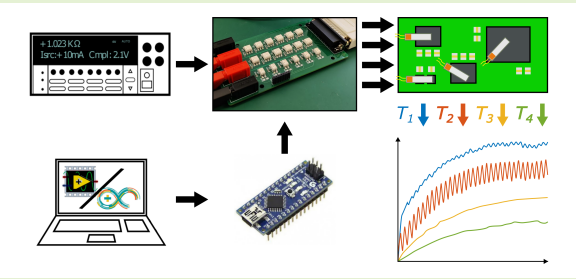

***Index Terms*— Microcontrollers, Measurement errors, Optical relays, Remote sensing, Switching systems**

I. Introduction

With the ongoing development of new technologies, it is becoming ever more necessary to measure multiple devices in either parallel applications or in sensor monitoring applications. With excessive heat or humidity, the quality and longevity of newly developed technologies can degrade if proper monitoring and control of the operating conditions are not implemented [1], [2]. Aside from electronic devices, the environmental quality within a working environment for both workers or systems must also be monitored in industrial settings to ensure a suitable and safe workplace is maintained. In such scenarios, multiple temperature, humidity or gas sensors can be used to monitor the quality of the environment although using multiple sensors can introduce complications if the appropriate circuitry is not properly implemented [3]–[5].

Typically, the temperature measurements of ICs in high-powered systems are performed using thermal imaging cameras although these measurements are only performed once and do not provide a continuous monitoring system that is also portable [6], [7]. Following this, the monotonic increase in operating frequency and switching speeds of emerging ICs now drives a need to monitor the temperature of multiple components in the newest generation PCBs [6], [8]. To provide continuous monitoring of a system, a compact, fast and accurate switching system is needed that can monitor multiple sensors.

Switching systems have demonstrated their utility in wireless temperature sensing for industrial applications [9], air quality monitoring through multichannel ozone monitoring systems [10], pH sensors for monitoring bacteria metabolism [11], agricultural crop growth monitoring using RFID communication [12] and wafer-scale characterization of superconducting ICs [12], [13]. Further to this, there are also demonstrations of wireless multichannel sensing systems that have significant benefits in wide area outdoor applications [14]–[16].

Despite developing a monitoring system with a low delay between sensor measurements, the development of a wireless sensing system necessitates an equally complex timing correction circuitry in order to allow a cascaded array of measurements in workplaces and there is a current push to minimize the costs of such systems. Further to excessive costs, significant care must be taken when monitoring and recording the data from multiple wireless sensors to ensure that the mea-

The work of Luke J. Bradley (corresponding author: Luke.Bradley@strath.ac.uk) and Nick G. Wright was with the School of Engineering at Newcastle University, England. Luke J. Bradley is now with the Rolls Royce UTC at the University of Strathclyde, Glasgow. The work of both authors was supported through the UK EPSRC Future Metrology Hub through the award EP/P006930/1.

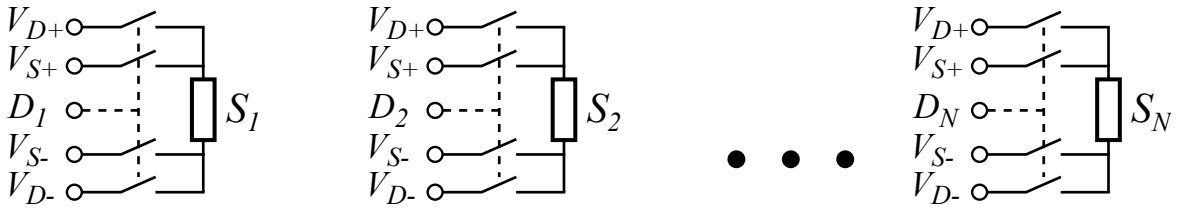

Fig. 1: Switching setup typically used to sequentially measure an array of sensors

surement times are synchronized and do not indicate spurious trends [17]–[19]. Despite presenting sub-1 ms measurement synchronization of multiple sensors, each of these techniques requires an optimized application-dependent synchronization system that will require re-calibration for alternative setups which greatly increases the complexity of inherently simple sensors. From previous works, both an academic and industrial requirement for a multichannel switching system can be seen, yet there has yet to be a fast, compact and cost-effective method for measuring smaller quantities of devices at a greater speed.

Here, an ORSS that can be interfaced with any benchtop sourcemeter/multimeter to sequentially measure multiple sensors is presented. The ORSS uses COTS optical-relay ICs to achieve a fast and low noise switching time within a small form factor. To highlight any parasitics introduced from the ORSS, a range of fixed-value resistors, capacitors and diodes are measured using a Keithley 2110 multimeter and a Keithley 2410 sourcemeter with and without the ORSS. To benchmark the switching speed of the ORSS, the switching speed of the ORSS with an Arduino Nano and a Keithley digital I/O are measured against the switching speed of a Keithley 7002 switching system. After finding the optimal control topology for the ORSS, the system is demonstrated through measuring the temperature profile of a microcontroller PCB using five PT1000 resistive temperature sensors.

II. Methodology

To sequentially measure an array of sensors, each sensor must be connected to the 4 test leads of a sourcemeter/multimeter independently whilst also remaining isolated from each other. The required setup for this can be seen in Fig. 1. For each sensor S, a digital switching signal D drives four switches connecting two switches to the positive terminal of the sensor and two to the negative terminal. When applying a driving voltage to a sensor (V_D), the measured sensing voltage (V_S) is used in a feedback loop to the sourcemeter/multimeter to remove the voltage drops caused by the parasitic cable resistances. Now, each sensor can be measured individually using separate digital signals to drive each set of switches.

In an ideal system, the switches depicted in Fig. 1 switch in zero time with no resistive losses. In reality, each switch will have an internal resistive loss and a delay associated with the switching propagation delay and these are common figures of merit that are listed for commercial switching systems. As such, the switching time and the on-state losses of the switches must be minimized in order to develop a fast and compact switching system.

III. Optical-Relay Switching System

The ORSS fabricated from COTS components can be seen in Fig. 2 with the equivalent circuit diagram of a single channel. To reduce the number of switches, the V_{D-} connection of each sensor channel is connected together. The ORSS can interface the input/output terminals of any sourcemeter/multimeter to 6 individual devices in a 2-wire or 4-wire configuration. For the three optical-relay switches, a 2 A G3VM-101DR1 and two 0.12 A G3VM-351E optical MOSFET relays for driving and sensing signals were used to ensure fast switching times of ∼0.1 ms. To drive the optical relays, a minimum switching current of 1 mA is needed to drive internal LEDs. Here, the ORSS is switched using the 3.3 V signals from an Arduino Nano and a Keithley 2110 multimeter, although the low driving currents ensures that it can be switched using any digital controller including C2000 microcontrollers, Raspberry Pi microcontrollers or FPGA families providing all can support DC output currents of 1 mA.

For conventional sourcemeters/multimeters, the sensing inputs leads are high impedance and have an ideally zero current draw when sensing, as such, two lower current switches can be used for the sensing signals and a single high current switch is only required for the driving signal. The optical relays ensure fast switching times whilst also providing isolation from the

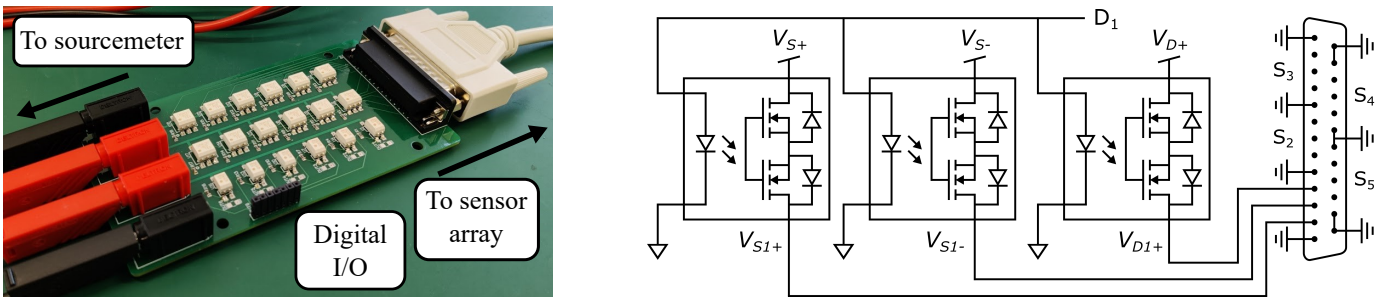

Fig. 2: ORSS PCB (left) and a single channel equivalent circuit diagram (right).

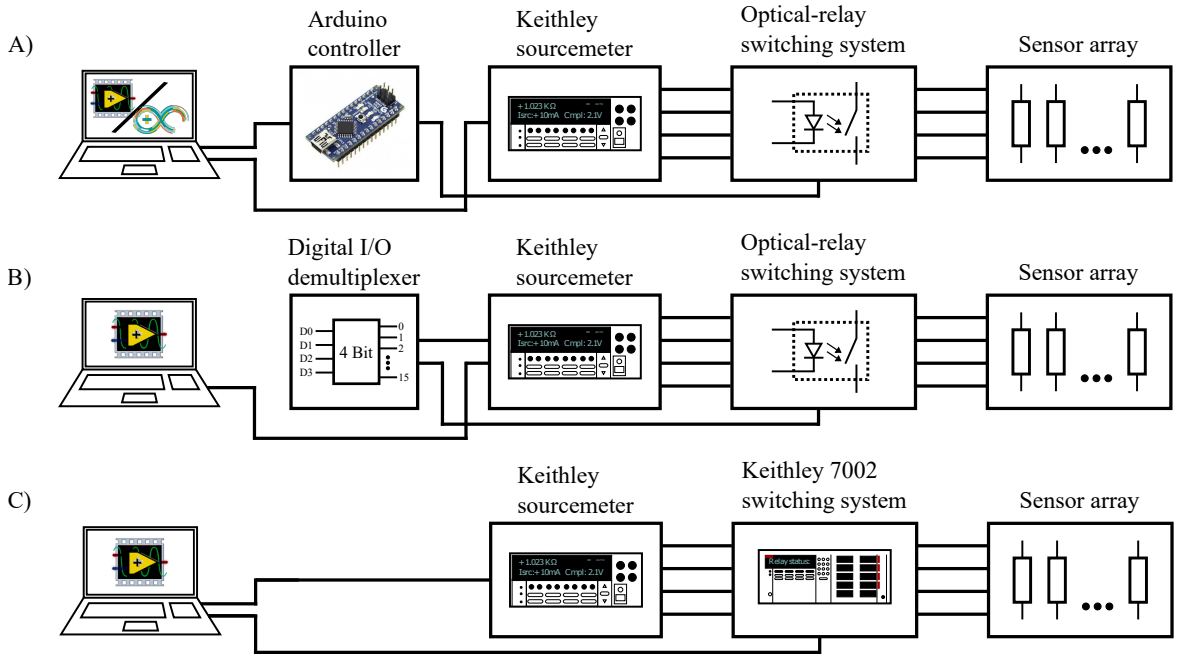

Fig. 3: The two ORSS switching topologies and the Keithley 7002 switching topology.

digital input signals from the board. For a single channel, a single driving signal is needed to drive the three optical relay switches. Using a single digital signal to switch three optical relays reduces the overall switching time. By using COTS components, the total cost of the ORSS with the PCB is less than £30 and will reduce further with larger orders.

IV. Sequential switching and sensor measurement system

To compare the maximum measurement speeds and accuracy of the ORSS developed here with commercial solutions, three switching topologies were investigated as illustrated in Fig. 3. In the three topologies, the parasitics introduced from the switching systems will affect the system measurement accuracy whilst the digital system used to control each system will affect the overall measurement speed. In topology A, an Arduino Nano microcontroller is used to generate the digital signal sent to the switching circuit. The Arduino Nano was programmed to use the same break-before-make strategy that is used by the Keithley 7002 switch system. Topology B is the same as topology A although the digital signal is generated from the digital output from a Keithley 2410 sourcemeter. For the 2410 sourcemeter, 4 general-purpose input/output pins can be used for controlling the switching system as described within the instruments datasheet. A 4 to 16-line decoder IC was used to increase the number of digital signals. In topology C, the commonly used 7002 topology is used to measure an array of devices and this topology is used as the benchmark for the ORSS. In all instances, all the equipment is controlled using a Serial interface with LabVIEW at the maximum available baud rate for each piece of equipment.

V. ORSS accuracy

Aside from switching/measurement delays, the introduction of a fast switching system could introduce non-negligible parasitic resistances, inductances and capacitances to the measurement of a sensor. Within the datasheets of the G3VM optical relays, the parasitic capacitance of both relays is 0.8 pF whilst the series resistance is 0.2 and 35 Ω for the 101DR1 and the 351E. An error of 0.8 pF is well below the parasitics of conventional sensors and FETs and the parasitic series resistance is removed by using the 4-terminal configuration depicted 1. Despite this, the PCB of the ORSS that contains the relays and their digital driving signals could introduce parasitic capacitance and crosstalk onto the device measurements signals and this must be accounted for.

The introduction of the ORSS PCB and relays will introduce parasitic capacitance, inductance and resistance to the sensor/DUT measurements. The remote sensing terminals of the sourcemeter will negate the effects of series resistance but the parasitic inductance and capacitance of the ORSS PCB and its components will effect the measurements. The parasitic capacitance from the microstrip PCB traces can be calculated from [20]

$$C_{par} = \frac{\epsilon_r l}{60\sqrt{\epsilon_0 \mu_0}\left[\frac{8h}{w} + \frac{w}{4h}\right]} \tag{1}$$

whilst the inductance is given by [21]

$$L_{par} = 60l\sqrt{\epsilon_0 \mu_0}\left[\frac{8h}{w} + \frac{w}{4h}\right] \tag{2}$$

where ϵ_0 and ϵ_r are the permittivity of free space and the relative permittivity of the conducting medium, μ_0 is the permeability of free space, l and w are the trace length and width, and h is the PCB thickness. Based on (1) and (2), the parasitic capacitance and inductance of the PCB traces is 0.386 pF/cm and 7.37 nH/cm. Considering the trace lengths within the PCB and the connections to the DUT, the parasitics introduced from the solid state relays is negligible in comparison to the total parasitics introduced from the PCB traces.

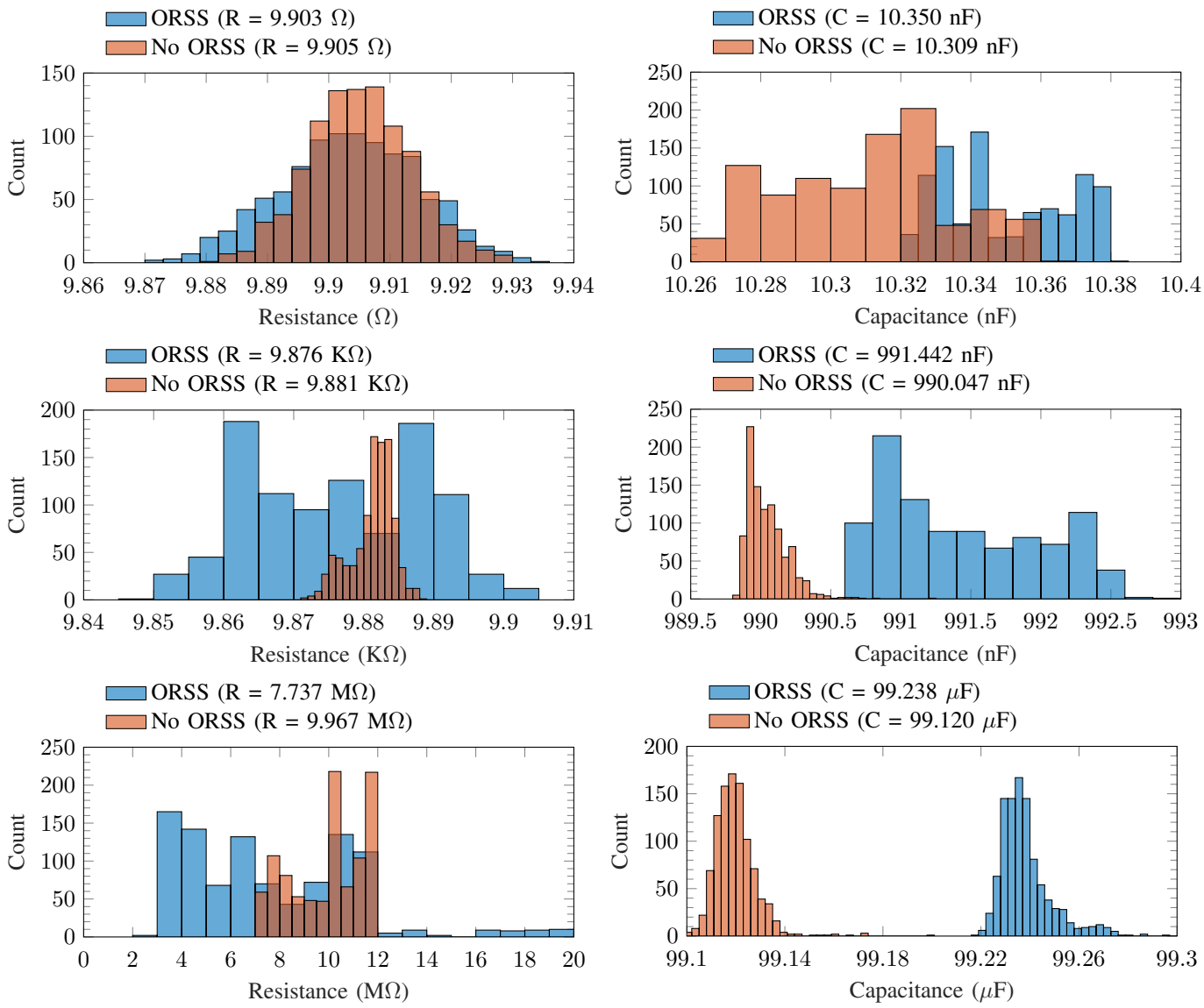

Fig. 4: Histogram plots of the 10 Ω, 10 KΩ and the 10 MΩ resistors and the 10 nF, 1 μF and the 100 μF capacitors.

To quantify the parasitics introduced from the ORSS, a 2110 multimeter was used to perform 1000 resistance measurements on a 10 Ω, 10 KΩ and a 10 MΩ resistor as well as 1000 capacitance measurements on a 10 nF, 1 μF and a 100 μF capacitor with and without the ORSS. A histogram of the measured resistances and capacitances in plotted in Fig. 4. In the case of the 10 MΩ resistor, the noise introduced from the ORSS significantly affects the average resistance producing a 38.8% error and resulting in measured resistances ranging from 2-20 MΩ, although it can also be seen that the measurements from the Keithley 2110 multimeter without the ORSS range from 7 to 12 MΩ suggesting that the resistance reaches the limitations of the multimeter. For all other measurements, an excellent agreement can be seen for each device resistance or capacitance resulting in less than 0.4% introduced from the ORSS. The significant error and spread in resistance values for the 10 MΩ measurements is a result of the Keithley 2110 multimeter accuracy in the 100 MΩ range. Within the datasheet of the multimeter, the resistance measurement error in the 100 MΩ range is quoted to be 2% although this is measured at an NPLC of 10. By using the an NPLC of 0.1 to achieve a fast measurement rate, any noise that is present during the resistance measurement is not filtered and perturbs the measured values. The noise is worsened in the case of using the ORSS as the low current/voltage noise generated within the PCB will distort measurements of devices with high resistance. For resistance values at or below 10 KΩ or capacitors ranging from 10 nF to 100 μF, the fast NPLC setting of the multimeter used with the ORSS produces minimal measurement error.

To see if noise generated from the ORSS will impinge device measurements of a non-linear device, 1000 IV sweeps were performed on a 1N4001 and a 1N5401 diode using a Keithley 2410 sourcemeter with and without the ORSS. The extracted threshold voltage and the dynamic resistance of each plot can be seen in Fig. 5 using the technique described in [22]. Once again, there is an excellent agreement between the extracted threshold voltage and resistance of the diodes

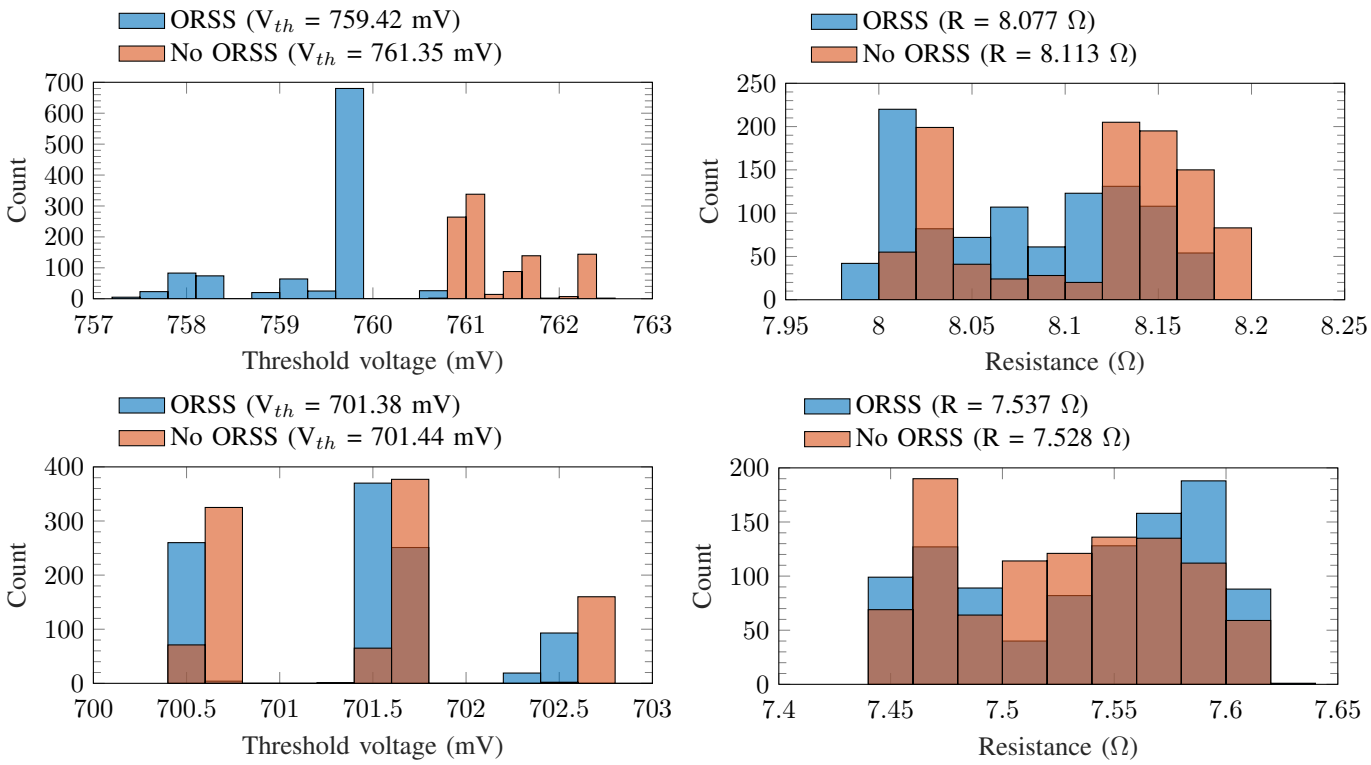

Fig. 5: Histogram plots of the threshold voltage and dynamic resistance of the 1N4001 (left) and the 1N5401 (right) diodes.

with and without the ORSS resulting in less than a 0.7% difference for all measurements.

VI. ORSS vs Keithley 7002 switching speed

From Sec V, the ORSS was demonstrated to have a negligible impingement on any device measurements with resistances below 10 KΩ and produced less than a 0.7% deviation in the extracted threshold voltage and resistance of COTS diodes. As well as accuracy, the ORSS must demonstrate a negligible switching delay between multiple sensors in order to maximise measurement speed within an array system.

To compare the switching speeds of the three topologies, a 5 V signal was sourced from the V_{D+} and the V_{D-} terminals of a Keithley 2410 sourcemeter. The outputs of the three topologies were measured using a RIGOL DS1074Z oscilloscope and the switching systems were controlled using LabVIEW and the recorded waveforms can be seen in Fig. 6. When controlling each switching system remotely, it can be seen that the switching delay from topology A that uses Arduino Nano is minimal with a pulse width of 345 μs whilst the switching delay from topology B and C are over 10 times slower with switching delays of 3.93 ms and 16.6 ms respectively. Of the three topologies, topologies A and C use a break-before-make approach which ensures that all switches or opened before closing the next channels and results in a delay between the switching of each channel. Despite the break-before-make delay within the Arduino Nano output signal, the switching delay between each channel of the Arduino Nano-controlled ORSS is the lowest of the three switching topologies. As covered in Sec VII, the fast switching speed of the Arduino Nano controlled ORSS is due to the greater baud rate of the Arduino Nano of 115200, whilst the Keithley digital I/O the Keithley 7002 is limited to respective baud rates of 57600 and 9600.

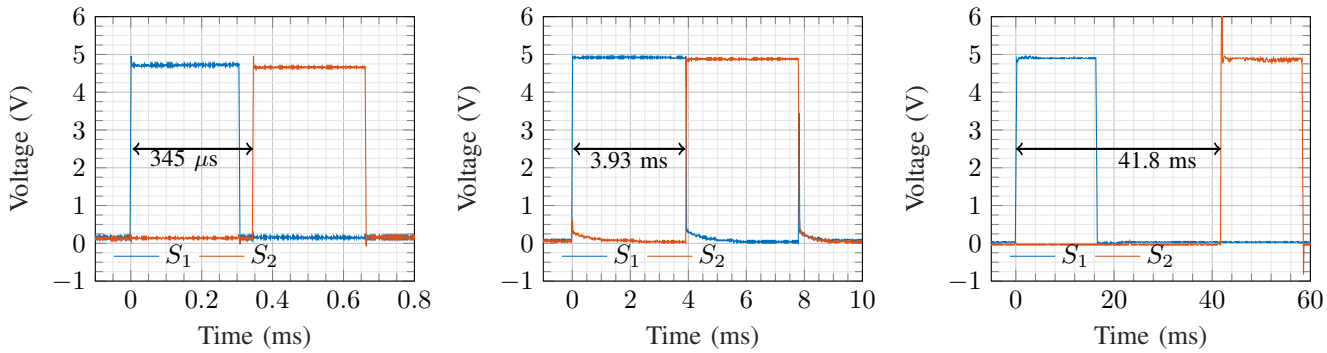

Fig. 6: Measured switching delays from topology A (left), B (middle) and C (right)

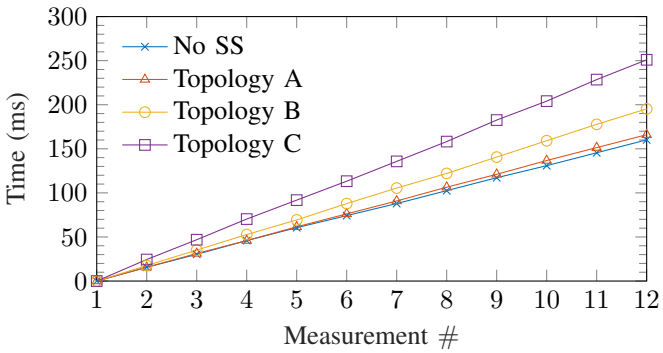

Fig. 7: Total measurement time for each topology compared to no switch system (No SS).

VII. Maximum Switching System Measurement Rate

As described in Sec. II, an ideal switching system will have zero switching speed and the overall measurement speed of any topology should be limited by the measurement speed of the sourcemeter/multimeter. To determine if the ORSS significantly hinders the maximum measurement speed of a measurement system, a Keithley 2410 sourcemeter was configured to measure a PT1000 resistive sensor 12 times. After this, the sourcemeter was connected to 12 different PT1000 sensors through topologies A-C). For topology A) and B), two ORSS boards were connected to the sourcemeter. Following guideline's within the Keithley 2410 manual, the sourcemeter was controlled remotely with the maximum equipment baud rate of 57600 and was configured to use 0.1 power lines cycles per measurement, triggered measurements and no auto-zero correction.

The time stamp for each resistance measurement can be seen in Fig. 7. Consistent with the switching delay measurements, it can be seen that the topologies using the Arduino Nano and the Keithley Digital I/O with the ORSS are significantly faster than the Keithley 7002 topology. Without any switching system, the measurement rate of the Keithley 2410 sourcemeter is 14.4 ms/measurement. For topologies A-C), respective measurement delays of 15.07, 17.74 and 22.67 ms/measurement were measured corresponding to maximum measurement rates of 66.35, 56.37 and 44.11 samples/s. The data highlights the favourability of using the ORSS compared to the Keithley 7002 switching system as it offers a much faster measurement rate and this is maximised by utilising a microcontroller to provide the switching driving signal.

VIII. Sequential Multichannel Sensing Demonstration

The demonstration setup for the multichannel sensing system can be seen in Fig. 8 along with the recorded temperature profiles. On the Uno, a PT1000 was thermally anchored to the 3.3 V and 5 V voltage regulators, the ATmega16u2 and ATmega328p microcontrollers and the PCB using GE varnish. The PT1000 temperature sensors were calibrated in accordance with the methodology presented in [23] and each sensor was measured using Topology A. The temperature sensors measured the heat generated from each IC on the board for a period of 9 minutes before power was disconnected.

In the first demonstration, to observe a significant change in Component/PCB temperature, the Arduino Uno was programmed to compute a complex mathematical operation for 8 seconds before entering a power-down sleep mode for 8 seconds. An internal watchdog timer was used to wake the microcontroller. In the second demonstration, five 150 Ω resistors were added to digital pins 2-5 which were driven high during the wake phase and low during the power-down

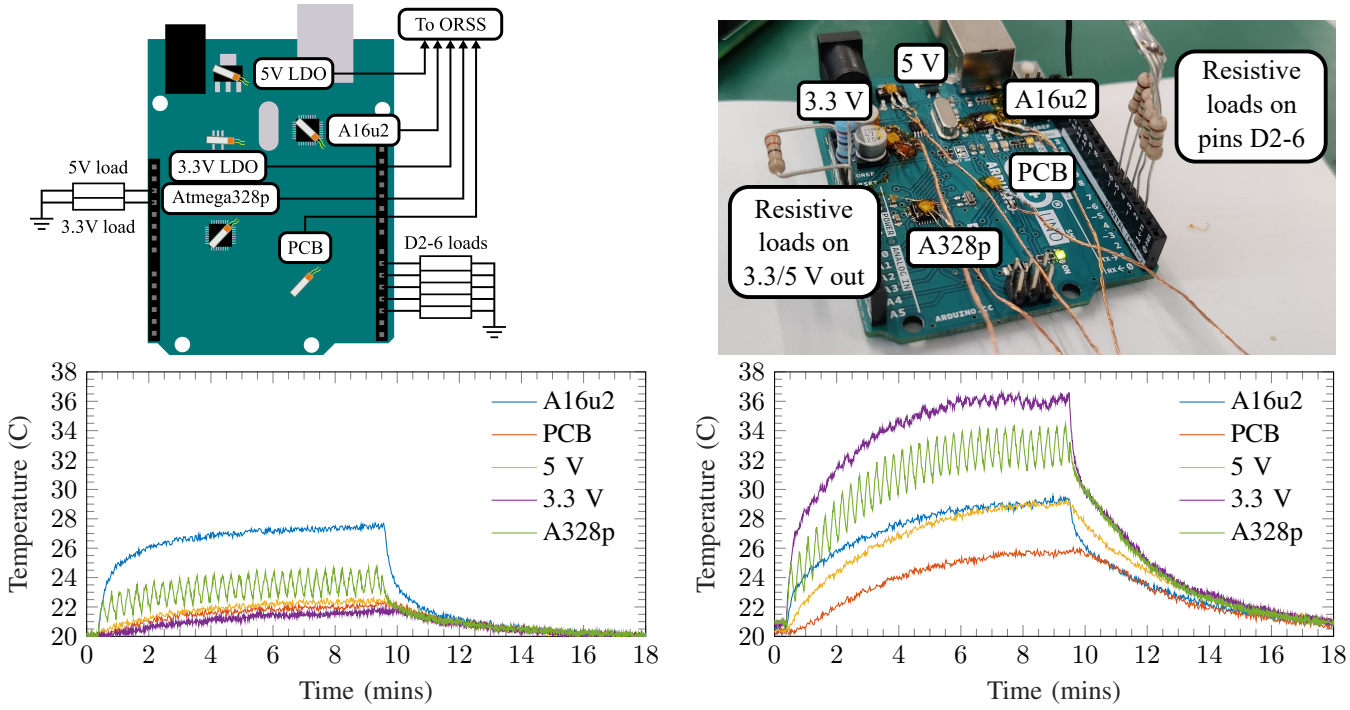

Fig. 8: ORSS multichannel resistive temperature measurement demonstration with PT1000 calibration.

sleep mode. Coupled with this, a 27 Ω and a 33 Ω resistive load were added to the output pins of the 3.3 V and 5 V voltage regulators respectively. After 9 minutes, the power was disconnected from the Arduino Uno to see how the boards cooled.

From the data, a clear increase in the components and the PCB temperature is observed when the restive loads are added to the system. In both runs, a clear sawtooth temperature pattern was measured for the ATmega328p microcontroller coinciding with the 8 second wake and deep-sleep cycles. The ATmega16u2 is used for USB/Serial communication and although it heats during operation there is no significant change in the temperature profile between both runs. Comparing the temperature profiles of the 3.3 and 5 V regulators, there is a significantly greater temperature rise to 36 C for the 3.3 V regulator compared to the 28 C reached by the 5 V regulator and this is attributed to the larger heat-sink packaging of the regulator's IC. After the power is disconnected, the second run took more than twice the time to return to the starting temperature.

From the data, the noise within the system introduces 0.4 C of noise to the temperature measurements. Here, we use an optimal NPLC value of 0.1 to satisfy both measurement speed and accuracy, although, for longer time scales, the NPLC can be increased to reduce noise. Although the PT1000 is used to measure a relatively small temperature range here, the PT1000 can measure temperatures of 60 to 800 K [24]. For temperatures ranging from 60 to 800 K, the correlating PT1000 resistance measured by the multimeter will be from 127 Ω to 3.16 KΩ with less than 0.4% error as covered in Sec. V. Despite the noise presented from the measurement demonstration, the ORSS was capable of recording the temperature profile of multiple components on the board over a run time of 18 minutes.

IX. Further refinements and future work

Using topology A, the ORSS can be used with a Keithley 2410 sourcemeter to achieve measurement speeds of up to 66.35 samples/s. In the case of the sourcemeter used here, the ORSS reduces the overall measurement speed by 4.4%. Although the delay from the ORSS is negligible here, this will become more significant if a faster sourcemeter/multimeter is used. Due to the limited measurement speed of the Keithley 2410 multimeter, the parasitic elements of the GV3M optical relays can be ignored. If a faster sourcemeter/multimeter is used, the parasitic input/output of the relays can become an issue and must be considered for faster measurement systems.

Throughout this work, the Arduino Nano and the Keithley 2410 and the Keithley 7002 were controlled remotely through LabVIEW with baud rates of 115200, 57600 and 9600 respectively. Based on the commands strings and the communication speed of each, a delay of 347.2 μs, 2.26 ms and 13.54 ms is incurred is incurred during each measurement. Despite utilising the techniques described throughout this work, the overall measurement speed is limited by the PC/equipment communication speed and the measurement speed of the sourcemeter/multimeter. This can be mitigated by using systems that can support higher baud rates, or by using equipment that can support superior communication protocols such direct USB or PCI express communication [25], [26]. As the Arduino Nano controlled ORSS reduced the maximum measurement rate of 4.4%, the overall system measurement speed can be increased by using a faster sourcemeter/multimeter or one with a faster communication speed than a 57600 baud rate.

X. Conclusion

A sub £30 optical relay switch system has been developed that can be used with a Keithley 2410 sourcemeter to achieve measurement speeds of 66.35 samples/s. The optical relay switch system can provide 2-wire or 4-wire measurements and is controlled using a single-wire digital interface. To quantify the error introduced by using the optical relay switch system, three resistors, three capacitors and two diodes were measured using a Keithley multimeter and sourcemeter with and without the optical relay switch system. Less than a 0.4% difference between the data measured with and without the optical relay switch system for resistance values below 10 KΩ and capacitance values from 10 nF to 100 μF was found. Similarly, less than 0.7% was found between the extracted threshold voltages and resistances of the two diodes when measured with and without the optical relay switch system. After further analysis of the system, it was found that the high measurement error at higher resistive loads ($>$ 1 MΩ) can be improved by reducing parasitics with the optical relay switch system printed circuit board.

Three switching topologies were compared to determine the optimal topology for the optical relay switch system. For each topology, a Keithley 2410 measured the output sensors and the switching was performed by an Arduino nano controlled optical relay switch system, a Keithley 2410 digital output controlled optical relay switch system and a conventional Keithley 7002 switch system. The Arduino nano controlled switch system demonstrated the fastest switching speed of 345 μs which was 11.4 times greater than the Keithley digital output controlled optical relay switch system and 121 times faster than the conventional Keithley 7002 switching system.

When using the optimal sourcemeter settings with the Arduino Nano controlled optical relay switch system, a peak measurement rate of 15.07 ms/measurement was achieved that correlates to a maximum sample measurement rate of 66.35 samples/s and can theoretically go as high as 2800 samples/s with a faster multimeter/sourcemeter. In demonstrating an example application, five PT1000 temperature sensors were thermally anchored to an Arduino Uno and were capable of accurately monitoring the temperature profile of the individual components and the printed circuit board.

With the work presented here, the framework for developing a multichannel switching system that can be used to monitor multiple sensors has been developed and characterized. Although the measurements and analysis herein are focused on the Keithley 2410 sourcemeter and the Arduino Nano, the optical relay switch system has been designed with universality in mind and so can be interfaced with any measurement system with remote sensing and any controlled by any digital microcontroller. Using the optical relay switch

system presented here, a cost-effective and versatile system for interfacing multiple sensors with measurement equipment has been presented negating the need for multiple measurement equipment and maximizing the sensing capabilities in workplaces and industry.

References

[1] Y. Gu, Y. Wang, J. Chen, B. Chen, M. Wang, and X. Zou, "Temperature-Dependent Dynamic Degradation of Carbon-Doped GaN HEMTs," *IEEE Transactions on Electron Devices*, vol. 68, no. 7, 2021, DOI: 10.1109/TED.2021.3077345.

[2] K. Ho, M. Wei, E. H. Sargent, and G. C. Walker, "Grain Transformation and Degradation Mechanism of Formamidinium and Cesium Lead Iodide Perovskite under Humidity and Light," *ACS Energy Letters*, vol. 6, no. 3, pp. 934–940, 2021, DOI: 10.1021/acsenergylett.0c02247.

[3] H. Jin, J. Yu, D. Cui, S. Gao, H. Yang, X. Zhang, C. Hua, S. Cui, C. Xue, Y. Zhang, Y. Zhou, B. Liu, W. Shen, S. Deng, W. Kam, and W. Cheung, "Remote Tracking Gas Molecular via the Standalone-Like Nanosensor-Based Tele-Monitoring System," *Nano-Micro Letters*, vol. 13, no. 1, 2021, DOI: 10.1007/s40820-020-00551-w.

[4] T. Rahman, Y. Xu, and Z. Qu, "Continuous-Domain Real-Time Distributed ADMM Algorithm for Aggregator Scheduling and Voltage Stability in Distribution Network," *IEEE Transactions on Automation Science and Engineering*, vol. 19, no. 1, pp. 60–69, 2022, DOI: 10.1109/TASE.2021.3072932.

[5] Y. Wang, S. Li, W. Ni, D. Abbott, M. Johnson, G. Pei, and M. Hedley, "Cooperative Localization and Association of Commercial-Off-the-Shelf Sensors in Three-Dimensional Aircraft Cabin," *IEEE Transactions on Automation Science and Engineering*, pp. 1–12, 2021, DOI: 10.1109/TASE.2021.3124207.

[6] A. Bauer, B. H. Zacher, and C. Schumann, "Enhanced Cooling of Multilayer PCB Motor Windings Using Thermal Vias," in *IECON 2021 – 47th Annual Conference of the IEEE Industrial Electronics Society*, 2021, pp. 1–5, DOI: 10.1109/IECON48115.2021.9589724.

[7] S. Wei, L. Ye, Z. Shaokun, and S. Qibiao, "Optimal Design of PCB Layout Based on Thermal Analysis Using Taguchi Method," in *2021 3rd Asia Energy and Electrical Engineering Symposium (AEEES)*, 2021, pp. 198–202, DOI: 10.1109/AEEES51875.2021.9403195.

[8] D. Koch, A. Sharma, J. Weimer, M. Weiser, T. Huesgen, and I. Kallfass, "A 48 V, 300 kHz, High Current DC/DC-Converter Based on Paralleled, Asymmetrical amp; Thermally Optimized PCB Embedded GaN Packages with Integrated Temperature Sensor," in *2021 33rd International Symposium on Power Semiconductor Devices and ICs (ISPSD)*, 2021, pp. 383–386, DOI: 10.23919/ISPSD50666.2021.9452241.

[9] G. Bruckner and J. Bardong, "Wireless Readout of Multiple SAW Temperature Sensors," *Sensors*, vol. 19, no. 14, 2019, DOI: 10.3390/s19143077.

[10] J. M. Barcelo-Ordinas, J. Garcia-Vidal, M. Doudou, S. Rodrigo-Muñoz, and A. Cerezo-Llavero, "Calibrating Low-Cost Air Quality Sensors Using Multiple Arrays of Sensors," in *2018 IEEE Wireless Communications and Networking Conference (WCNC)*, 2018, pp. 1–6, DOI: 10.1109/WCNC.2018.8377051.

[11] C. Ocaña, S. Brosel-Oliu, N. Abramova, and A. Bratov, "Low-cost multichannel system with disposable pH sensors for monitoring bacteria metabolism and the response to antibiotics," *Instrumentation Science & Technology*, vol. 49, no. 3, pp. 288–303, 2021, DOI: 10.1080/10739149.2020.1828097.

[12] R. Rayhana, G. Xiao, and Z. Liu, "RFID Sensing Technologies for Smart Agriculture," *IEEE Instrumentation Measurement Magazine*, vol. 24, no. 3, pp. 50–60, 2021, DOI: 10.1109/MIM.2021.9436094.

[13] J. T. West, A. Kurlej, A. Wynn, C. Rogers, M. A. Gouker, and S. K. Tolpygo, "Wafer-Scale Characterization of a Superconductor Integrated Circuit Fabrication Process, Using a Cryogenic Wafer Prober," *IEEE Transactions on Applied Superconductivity*, vol. 32, no. 5, pp. 1–12, 2022, DOI: 10.1109/TASC.2022.3172660.

[14] P. Gil, E. Smyk, R. Gałek, and Łukasz Przeszłowski, "Thermal, flow and acoustic characteristics of the heat sink integrated inside the synthetic jet actuator cavity," *International Journal of Thermal Sciences*, vol. 170, p. 107171, 2021, DOI: 10.1016/j.ijthermalsci.2021.107171.

[15] H. M. E. Hussein, M. Rinaldi, M. Onabajo, and C. Cassella, "A chipless and battery-less subharmonic tag for wireless sensing with parametrically enhanced sensitivity and dynamic range," *Scientific Reports*, vol. 11, no. 1, pp. 1–11, 2021, DOI: 10.1038/s41598-021-82894-x.

[16] H. Zhang, R. Srinivasan, and V. Ganesan, "Low Cost, Multi-Pollutant Sensing System Using Raspberry Pi for Indoor Air Quality Monitoring," *Sustainability*, vol. 13, no. 1, 2021, DOI: 10.3390/su13010370.

[17] T. Yang, Y. Niu, and J. Yu, "Clock Synchronization in Wireless Sensor Networks Based on Bayesian Estimation," *IEEE Access*, vol. 8, pp. 69 683–69 694, 2020, DOI: 10.1109/ACCESS.2020.2984785.

[18] G. Coviello and G. Avitabile, "Multiple Synchronized Inertial Measurement Unit Sensor Boards Platform for Activity Monitoring," *IEEE Sensors Journal*, vol. 20, no. 15, pp. 8771–8777, 2020, DOI: 10.1109/JSEN.2020.2982744.

[19] T. Steinmetzer, S. Wilberg, I. Bönninger, and C. M. Travieso, "Analyzing gait symmetry with automatically synchronized wearable sensors in daily life," *Microprocessors and Microsystems*, vol. 77, p. 103118, 2020, DOI: 10.1016/j.micpro.2020.103118.

[20] C. R. Paul, *Analysis of multiconductor transmission lines*, ser. IEEE. John Wiley & Sons, 2007.

[21] ——, *Inductance: Loop and Partial*, ser. IEEE. John Wiley & Sons, 2010.

[22] S. Sze and K. Ng, *Physics of Semiconductor Devices*, 3rd ed. Hoboken, NJ, USA: Wiley, 2007, DOI: 10.1002/0470068329.

[23] A. K. Saw, G. Channagoudra, T. Pethker, K. Gangadharan, and V. Dayal, "Automated low-temperature resistivity measurement setup: Design and fabrication," *Materials Today: Proceedings*, vol. 47, pp. 1670–1675, 2021, National Conference on Recent Advances in Functional Materials-2020, DOI: 10.1016/j.matpr.2021.05.341.

[24] Y. Qiu, Y. Zheng, B. Shen, N. Wang, G. Lei, T. Wang, H. Chang, and S. Shu, "Experimental investigation on the temperature and pressure characteristics of supercritical helium for liquid hydrogen pressurisation," *Journal of Energy Storage*, vol. 46, p. 103895, 2022, DOI: 10.1016/j.est.2021.103895.

[25] Q. D. Zhou, S. Yamada, P. Robbe, D. Charlet, R. Itoh, M. Nakao, S. Y. Suzuki, T. Kunigo, E. Jules, E. Plaige, M. Taurigna, H. Purwar, O. Hartbrich, M. Bessner, K. Nishimura, G. Varner, Y.-T. Lai, T. Higuchi, R. Sugiura, D. Biswas, and P. Kapusta, "PCI-Express Based High-Speed Readout for the Belle II DAQ Upgrade," *IEEE Transactions on Nuclear Science*, vol. 68, no. 8, pp. 1818–1825, 2021, DOI: 10.1109/TNS.2021.3086526.

[26] D. Das Sharma, "PCI Express 6.0 Specification: A Low-Latency, High-Bandwidth, High-Reliability, and Cost-Effective Interconnect With 64.0 GT/s PAM-4 Signaling," *IEEE Micro*, vol. 41, no. 1, pp. 23–29, 2021, DOI: 10.1109/MM.2020.3039925.

Luke J. Bradley is a Research Associate working within the Rolls Royce UTC group at the University of Strathclyde. He received his Bachelor of Engineering in Electrical and Electronic Engineering from Newcastle University in 2015, from which, he worked in the area of Cryogenic Power Electronics and received his PhD from Newcastle University in 2020. His research interests include power electronics and circuits at cryogenic temperatures, power device simulations and microcontroller data logging applications.

Nick G. Wright is Professor of Electronic Materials at Newcastle University UK and a Fellow of the Turing Institute. He received his Bachelor and PhD degrees from Edinburgh University. He has led major projects on power semiconductor devices, robotics and AI. He has authored over 200 papers, contributed to over 10 patents and made numerous conference presentations. His research interests include electronic materials, power devices, and the applications of materials to robotics and artificial intelligence – particularly for manufacturing and deep ocean exploration.